Is Langmuir Circulation Driven by Surface Waves or Surface Cooling?

MING LI AND CHRIS GARRETT

Centre for Earth and Ocean Research, University of Victoria, Victoria, British Columbia, Canada

(Manuscript received 7 December 1993, in final form 6 May 1994)

ABSTRACT

The ratio of the buoyancy force driving thermal convection to the surface wave vortex-force driving Langmuir circulation in the Craik–Leibovich mechanism involves the Hoenikker number Ho. The critical value Ho_c, at which wave forcing and thermal convection contribute equally to the circulation, is found to increase with decreasing Langmuir number La and approaches 3 in the small La limit. For a typical wind speed and surface cooling, Ho is of order $O(10^{-2})$ to $O(10^{-1})$. Thus, wave forcing dominates over thermal convection in driving Langmuir circulation.

Stratification induced by strong surface heating suppresses the circulation generated by wave forcing and could completely inhibit the CL instability. In the physically plausible range of $-0.1 < Ho < 0$, however, this does not happen for small La and the dynamical effect of heating is very small.

For a given heat flux, the temperature difference between the regions of surface divergence and convergence in Langmuir circulation depends on Ho, Pr, and La and on the depth distribution of the heating, but is typically $O(10^{-2})$ K.

1. Introduction

Langmuir circulation, consisting of a pattern of counterrotating vortices oriented downwind (Langmuir 1938), is a key process in the ocean surface layer, although its precise role in distributing heat, momentum, and gas in the layer remains to be determined (Thorpe 1985, 1992).

Observations of Langmuir circulation by Weller and Price (1988) showed a downward vertical velocity sometimes exceeding 0.2 m s^{-1} below the surface convergence. The downwind-directed current is greatest at the surface convergence and has a magnitude comparable to the downwelling velocity at middepth in the mixed layer. This downwind and downwelling flow is jetlike in structure, being confined to a narrow region in the crosswind direction. The temperature difference between the surface divergence and convergence is generally small, ranging between 0.005 and 0.015 K under strong winds (Thorpe and Hall 1982; Weller and Price 1988).

The currently accepted model of Langmuir circulation is the Craik–Leibovich (CL) model (Craik and Leibovich 1976; Craik 1977; Leibovich 1977), in which the Stokes drift of surface waves tilts the vertical vortex lines of a near surface downwind jet to produce streamwise vorticity with surface convergence at the jet maximum. The jet is then reinforced by continued acceleration, by the wind stress, of the converging surface flow. Li and Garrett (1993, hereafter LG), however, suggested that the CL model is incomplete as it predicts a weaker downwind jet than is observed.

Other suggested mechanisms for Langmuir circulation include thermal convection in a shear flow (Csanady 1965). This was later dismissed on the grounds that Langmuir circulation is observed under thermally stable or neutral conditions (Leibovich 1983). However, incoming solar radiation is distributed over an absorption depth so that water in a surface layer may still become unstable due to sensible and latent heat losses at the surface. Thus, thermal convection can occur even when the ocean receives a net heat flux, and can certainly occur if there is net heat loss.

In this paper, we add surface buoyancy forcing to the CL model of Langmuir circulation. We will assume that the convective cells have their axes aligned in the direction of the wind, as this is the preferred mode for the CL mechanism, and convective instability of a shear flow favors cells aligned in the wind direction but suppresses crosswind instability (Etling and Brown 1993; Domaradzki and Metcalfe 1988; Kuettner 1971; Kuo 1963). It will be shown that wave forcing in the CL mechanism dominates over thermal convection in driving Langmuir circulation.

2. Model formulation

The wind stress τ_w gives a surface boundary condition

Corresponding author address: Dr. Ming Li, University of Victoria, Centre for Earth and Ocean Research, P.O. Box 1700, Victoria, B.C. V8W 2Y2, Canada.

© 1995 American Meteorological Society

Unauthenticated | Downloaded 09/29/22 10:50 AM UTC

$$\tau_w = \rho_w \nu_T \frac{\partial \tilde{u}}{\partial \tilde{z}}, \tag{1}$$

where ρ_w is the water density, ν_T is the eddy viscosity, and $\tilde{u}$ is the downwind velocity. Similarly, a surface heat flux Q into the sea surface requires

$$Q = C_p \rho_w \kappa_T \frac{\partial \tilde{\theta}}{\partial \tilde{z}}, \tag{2}$$

where C_p is the specific heat at constant pressure, κ_T is the eddy diffusivity of heat, and $\tilde{\theta}$ is the temperature.

The wind stress τ_w is related to the wind speed U_w through

$$\tau_w = \rho_w u_*^2 = C_D \rho_a U_w^2, \tag{3}$$

where u_* is the water friction velocity, ρ_a is the air density, and C_D is the drag coefficient. Using a typical value of the drag coefficient, LG estimated

$$u_* = \left(\frac{1}{950} \text{ to } \frac{1}{650}\right) U_w \tag{4}$$

for wind speeds between 5 and 25 m s^{-1}.

The total surface heat flux Q has four components:

$$Q = Q_s - Q_b - Q_h - Q_e, \tag{5}$$

where Q_s is the rate of inflow of solar energy through the sea surface and is distributed over an absorption depth, Q_b is the net rate of heat loss by the sea as longwave radiation to the atmosphere, Q_h is the sensible heat flux, and Q_e the rate of heat loss by evaporation (latent heat flux). The last two terms, Q_h and Q_e, may be of either sign, depending on the turbulent properties of the atmosphere and can be calculated from measurements of temperature, humidity, and radiation using bulk aerodynamic formulas and transfer coefficients given as functions of stability and wind (Large and Pond 1982; Smith 1988). At night, the sensible, evaporative, and longwave radiative components usually combine to yield a net upward heat flux ($Q < 0$) that may reach as high as 200 to 500 W m^{-2} (Shay and Gregg 1986). During the day the ocean typically receives heat (i.e., $Q > 0$), though in winter the outgoing fluxes may overcome the incoming insolation to yield $Q < 0$ even during the daytime. We shall consider a period much shorter than the diurnal cycle, so that the heat flux is taken to be steady.

For a two-dimensional model of ocean surface water in a crosswind vertical section, the governing equations can be written as (Leibovich 1977)

$$\frac{\partial \tilde{u}}{\partial \tilde{t}} + \tilde{v}\frac{\partial \tilde{u}}{\partial \tilde{y}} + \tilde{w}\frac{\partial \tilde{u}}{\partial \tilde{z}} = \nu_T \nabla^2 \tilde{u}, \tag{6}$$

$$\frac{\partial \tilde{\Omega}}{\partial \tilde{t}} + \tilde{v}\frac{\partial \tilde{\Omega}}{\partial \tilde{y}} + \tilde{w}\frac{\partial \tilde{\Omega}}{\partial \tilde{z}} = \nu_T \nabla^2 \tilde{\Omega} - \frac{d\tilde{u}_s}{d\tilde{z}}\frac{\partial \tilde{u}}{\partial \tilde{y}} + \alpha g \frac{\partial \tilde{\theta}}{\partial \tilde{y}}, \tag{7}$$

$$\frac{\partial \tilde{\theta}}{\partial \tilde{t}} + \tilde{v}\frac{\partial \tilde{\theta}}{\partial \tilde{y}} + \tilde{w}\frac{\partial \tilde{\theta}}{\partial \tilde{z}} = \kappa_T \nabla^2 \tilde{\theta}, \tag{8}$$

$$\tilde{v} = -\tilde{\psi}_{\tilde{z}}, \quad \tilde{w} = \tilde{\psi}_{\tilde{y}}, \quad \tilde{\Omega} = \nabla^2 \tilde{\psi}, \tag{9}$$

in which $\tilde{y}$ is in a horizontal direction perpendicular to the wind and $\tilde{z}$ is vertically upward. The three velocity components $\tilde{u}$, $\tilde{v}$, $\tilde{w}$ represent the downwind, crosswind, and vertical velocities; $\tilde{\Omega}$ is the streamwise vorticity, $\tilde{u}_s$ is the Stokes drift current, and α is the coefficient of thermal expansion. Here we parameterize turbulence by constant eddy viscosity ν_T and constant eddy diffusivity κ_T. In the vorticity equation $(d\tilde{u}_s/d\tilde{z})(\partial\tilde{u}/\partial\tilde{y})$ is the Craik–Leibovich vortex force and $\alpha g(\partial\tilde{\theta}/\partial\tilde{y})$ represents the production of streamwise vorticity by buoyancy gradients, assuming net evaporation makes a small contribution to the surface buoyancy flux B_0 (e.g., Shay and Gregg 1986); that is, $B_0 \approx -\alpha g Q/(\rho_w C_p)$.

The Stokes drift current can be approximated adequately by an exponential profile in modeling Langmuir circulation (LG) so that we can take $\tilde{u}_s = 2S_0 \times \exp(2\beta\tilde{z})$ in which $2S_0$ is the surface drift and $1/(2\beta)$ is the e-folding depth of the Stokes drift.

Nondimensionalizing distance, velocities, time, and temperature as

$$(\tilde{y}, \tilde{z}) = \beta^{-1}(y, z), \tag{10}$$

$$\tilde{u} = \frac{u_*^2}{\nu_T \beta} u, \tag{11}$$

$$(\tilde{v}, \tilde{w}) = \frac{u_*^2}{\nu_T \beta}\left(\frac{\nu_T S_0 \beta}{u_*^2}\right)^{1/2}(v, w), \tag{12}$$

$$\tilde{t} = \frac{\nu_T}{u_*^2}\left(\frac{\nu_T S_0 \beta}{u_*^2}\right)^{-1/2} t, \tag{13}$$

$$\tilde{\theta} = \frac{Q}{C_p \rho_w \kappa_T \beta}\theta, \tag{14}$$

we obtain the following nondimensionalized governing equations

$$\frac{\partial u}{\partial t} + v\frac{\partial u}{\partial y} + w\frac{\partial u}{\partial z} = \text{La}\nabla^2 u, \tag{15}$$

$$\frac{\partial \Omega}{\partial t} + v\frac{\partial \Omega}{\partial y} + w\frac{\partial \Omega}{\partial z} = \text{La}\nabla^2\Omega - \frac{du_s}{dz}\frac{\partial u}{\partial y} - \text{Ho Pr}\frac{\partial \theta}{\partial y}, \tag{16}$$

$$\frac{\partial \theta}{\partial t} + v\frac{\partial \theta}{\partial y} + w\frac{\partial \theta}{\partial z} = \frac{\text{La}}{\text{Pr}}\nabla^2\theta, \tag{17}$$

$$v = -\frac{\partial \psi}{\partial z}, \quad w = \frac{\partial \psi}{\partial y}, \quad \Omega = \nabla^2\psi, \tag{18}$$

with the surface boundary conditions given by

$$\frac{\partial u}{\partial z} = 1, \quad \frac{\partial \theta}{\partial z} = 1, \quad \psi = \frac{\partial^2 \psi}{\partial z^2} = 0. \tag{19}$$

The nondimensionalized Stokes drift has a profile $u_s = 2e^{2z}$. There are three dimensionless parameters in

Unauthenticated | Downloaded 09/29/22 10:50 AM UTC

the above equations. The Langmuir number (Leibovich 1977)

$$\mathrm{La} = \left(\frac{\nu_T \beta}{u_*}\right)^{3/2} \left(\frac{S_0}{u_*}\right)^{-1/2} \tag{20}$$

represents the ratio of viscous to inertial forces. The Prandtl number $\mathrm{Pr} = \nu_T/\kappa_T$ is the ratio of eddy viscosity to eddy diffusivity. The third dimensionless number is the Hoenikker number,[1] which is defined as

$$\mathrm{Ho} = \frac{B_0}{S_0 \beta u_*^2}, \tag{21}$$

or

$$\mathrm{Ho} = -\frac{\alpha g Q/(C_p \rho_w)}{S_0 \beta u_*^2} \tag{22}$$

if the surface heat flux dominates the contribution to the surface buoyancy flux. It is noted that $\mathrm{Ho} > 0$ when the ocean loses heat ($Q < 0$) and $\mathrm{Ho} < 0$ when the ocean receives heat ($Q > 0$). The product Ho Pr represents the ratio of convective forcing to wave forcing through the Stokes drift. We can rewrite Ho as

$$\mathrm{Ho} = -\frac{4}{\kappa}\left(\frac{2S_0}{u_*}\right)^{-1} \frac{1/(2\beta)}{L} \tag{23}$$

in which $L = -u_*^3/(\kappa B_0)$ is the Monin–Obukhov length and κ is the von Kármán constant. The ratio D/L of the mixed layer depth to the Monin–Obukhov length has been used as a bulk stability parameter, indicating the importance of convective instability of the mixed layer when the parameter is large and negative (Turner 1973). This criterion relies on the assumption of a smooth surface and no coherent secondary flows and is not a priori applicable to the upper ocean, which contains breaking waves and Langmuir cells (Thorpe 1985).

Taking $\alpha = (1 \text{ to } 2) \times 10^{-4}\ \mathrm{K}^{-1}$ as for temperature in the range 10–20 K, $C_p = 4.0 \times 10^3\ \mathrm{J\ K^{-1}\ kg^{-1}}$, and using the estimates $u_* = (1/950 \text{ to } 1/650)U_w$, $2S_0 = (0.014 \text{ to } 0.015)U_w$, and $1/(2\beta) = 0.12U_w^2/g$ for fully developed seas (LG), we find

$$\mathrm{Ho} \approx -(7 \times 10^{-4})\frac{Q}{U_w}. \tag{24}$$

For a surface heat loss rate $Q = -200\ \mathrm{W\ m^{-2}}$ and a wind speed $U_w = 10\ \mathrm{m\ s^{-1}}$, Ho is thus estimated to be 0.014. The spectrum of the Stokes drift gradient $S_0\beta$ is flat so that Ho is fairly independent of fetch. If Pr = 1 is taken for turbulent fluids, then the convective forcing appears to be typically less than 2% of the Stokes drift forcing, provided that both $(du_s/dz)(\partial u/\partial y)$ and $\partial\theta/\partial y$ are of the same order of magnitude. Given the different profiles of the two forcing terms in (16), however, it remains to be seen whether Ho = 1 really does represent the transition from wave forcing (through Stokes drift) to convective forcing, or whether the transition occurs at some other value of Ho.

To investigate this, (15)–(18) together with (19) are solved numerically by a spectral code extended from that described by LG. A main point to make is that the stress-type boundary conditions for u and θ can be made homogeneous by the decomposition $u = U(z, t) + u'(y, z, t)$ and $\theta = T(z, t) + \theta'(y, z, t)$ in which

$$U(z, t) = 2(\mathrm{La}t)^{1/2} f(\eta), \quad \eta = \frac{z}{2(\mathrm{La}t)^{1/2}}, \tag{25}$$

$$T(z, t) = 2\left(\frac{\mathrm{La}}{\mathrm{Pr}}t\right)^{1/2} f(\zeta), \quad \zeta = \frac{z}{2(\mathrm{La}t/\mathrm{Pr})^{1/2}}, \tag{26}$$

$$f(\eta) = \pi^{-1/2} e^{-\eta^2} + \eta\ \mathrm{erfc}(-\eta). \tag{27}$$

The perturbations $u'(y, z, t)$ and $\theta'(y, z, t)$ are then stress-free and flux-free at the upper boundary, and we assume that this is also true at the lower boundary. Hence,

$$\frac{\partial u'}{\partial z} = \frac{\partial \theta'}{\partial z} = 0, \quad \psi = \frac{\partial^2 \psi}{\partial z^2} = 0 \quad \text{at} \quad z = 0, -\beta d, \tag{28}$$

in which d is the depth of the computational box.

The computation is carried out in a rectangular box, which has a horizontal extent L. Periodic boundary conditions are imposed at the two lateral boundaries; that is,

$$\psi(y + \beta L) = \psi(y), \quad u'(y + \beta L) = u'(y), \quad \theta'(y + \beta L) = \theta'(y). \tag{29}$$

The cells typically grow to fill the domain regardless of the size of βL. We shall choose a computational box with $\beta L = 2\pi$ and $\beta d = \pi$ in the following numerical simulations. For homogeneous water, the dependence of numerical results on the box size was discussed in LG. The maximum downwelling velocity, on which our main conclusion is based, appears to be a weak function of box size at small La. Although the vortex force of surface waves has a depth scale determined by the profile of the Stokes drift, neither the vortex force nor the buoyancy force have any inherent horizontal scale. It is therefore expected that the comparison of the two forcing terms will be independent of the box size once the box has a depth much greater than the depth scale of the vortex force. With $\beta L = 2\pi$ the Stokes drift drops to less than 0.002 of its surface value at the bottom boundary.

[1] The dimensionless number Ho is named after the distinguished ocean thermodynamicist Dr. Felix Hoenikker (Vonnegut 1963). Dr. Hoenikker, the inventor of *ice nine*, was modeled on Irving Langmuir, for whom Kurt Vonnegut's brother Bernard worked at the General Electric Laboratories in Schenectady, New York (B. Vonnegut 1994, personal communication).

Unauthenticated | Downloaded 09/29/22 10:50 AM UTC

Computer power has limited our simulations so far to 64 × 64 or 128 × 128 Fourier modes. For this, we have adequate resolution, with one-dimensional energy spectra showing exponential decay at high wavenumbers if La > 0.01. Time steps are chosen to ensure numerical stability. Generally speaking, higher resolution and a smaller time step are required at smaller La. For La = 0.01, the eddy viscosity $\nu_T = 2.6 \times 10^{-5} U_w^3/g$ so that for $U_w = 10$ m s^{-1}, $\nu_T = 2.6 \times 10^{-3}$ m^2 s^{-1}, close to the estimate given in Leibovich and Radhakrishnan (1977), although real flows may have La somewhat smaller than 0.01. However, the scale analysis to be discussed later will produce useful insights into the flow properties, even at smaller La which cannot be resolved by the numerical model.

3. Combined wave and thermal forcing

In this section we investigate the circulation driven simultaneously by wave and thermal forcing. The flows are studied in detail for a typical parameter set. Then how three key flow indices vary with the dimensionless parameters La, Ho, and Pr is investigated.

a. Flow and temperature fields

At small La vigorous cells are generated by wave forcing, so we question if the circulation will be significantly reinforced by the addition of a typically small convective forcing. We take Pr = 1, La = 0.02, and Ho = 0.05 and focus on the quasi-steady cells that emerge from the amalgamation of small cells.

Figure 1 shows the distributions of downwind current velocity, temperature, vorticity, and streamfunction over a vertical crosswind section. When Pr = 1, the temperature differs from the downwind current only in sign because both are advected by the same crosswind velocities v and w and satisfy the same boundary conditions. It is clear that u and θ have an extremum at the downwelling site. A surface boundary layer and a vertical boundary layer at the downwelling site are apparent. Within the narrow downwelling region, the vorticity jumps between the two extreme values. Away from the two boundary-layer regions, viscous dissipation is weak and u, θ, and Ω appear to be homogenized, as expected for flows within closed streamlines (Batchelor 1956; Rhines and Young 1982).

We investigate changes in key flow quantities from Ho = 0 to Ho = 0.05 at La = 0.02. The first is the maximum downwelling velocity $\tilde{w}_{\rm dn}$, which can be written as

$$\tilde{w}_{\rm dn} = u_* \left(\frac{S_0}{u_*}\right)^{1/3} {\rm La}^{-1/3} w_{\rm dn}, \tag{30}$$

using

$$\frac{\nu_T \beta}{u_*} = {\rm La}^{2/3} \left(\frac{S_0}{u_*}\right)^{1/3} \tag{31}$$

from (20). The second flow quantity is the pitch (the ratio of the surface downwind jet strength to the maximum downwelling velocity):

$${\rm Pt} = \frac{\tilde{u}_{\rm con} - \tilde{u}_{\rm div}}{\tilde{w}_{\rm dn}} = \left(\frac{S_0}{u_*}\right)^{-2/3} {\rm La}^{-1/3} \frac{u_{\rm con} - u_{\rm div}}{w_{\rm dn}}. \tag{32}$$

The third quantity to compare is the temperature difference between the divergence and convergence lines:

$$\delta\tilde{\theta} = \tilde{\theta}_{\rm div} - \tilde{\theta}_{\rm con} = \frac{S_0 \beta u_*}{\alpha g} \left(\frac{S_0}{u_*}\right)^{-1/3} {\rm Ho\ Pr\ La}^{-2/3} \delta\theta. \tag{33}$$

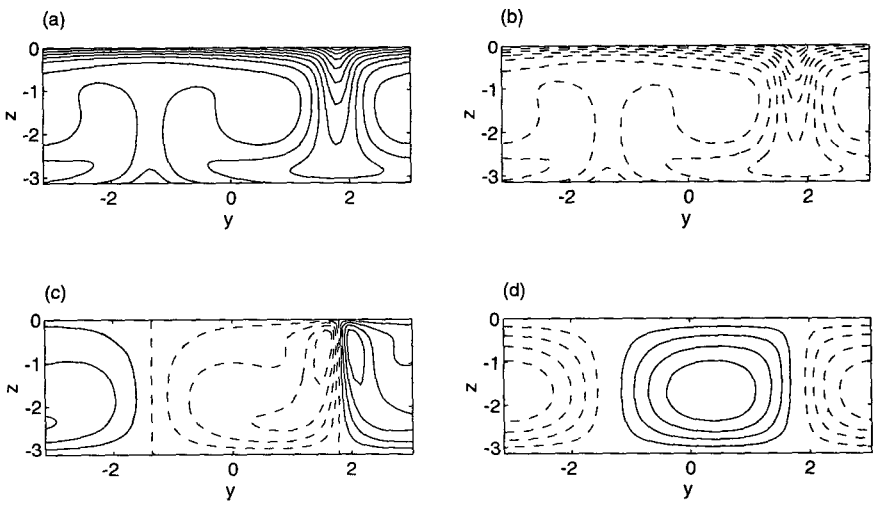

FIG. 1. Contours of flow fields for quasi-steady cells at La = 0.02, Ho = 0.05, and Pr = 1: (a) downwind current, (b) temperature, (c) streamwise vorticity, and (d) streamfunction.

Unauthenticated | Downloaded 09/29/22 10:50 AM UTC

We note that Ho = 0.05 corresponds to a fairly strong heat loss at moderate wind speeds. The maximum downwelling velocity is only 4% larger, representing a marginal increase in the circulation caused by the extra convective forcing. Without considering buoyancy, LG found that the pitch predicted by the Craik–Leibovich model is weaker than the observed value. The pitch at Ho = 0.05 is slightly less than that at Ho = 0. Water at the surface convergence is colder than that at the divergence; the temperature difference is estimated to be about 0.027 K using the same values of the parameters as used in estimating Ho in (24). For Ho = 0.014 found at typical oceanic conditions, the surface buoyancy forcing will have even less effect on Langmuir circulation, so that temperature is effectively a passive tracer and the temperature difference is linearly proportional to Q if the other parameters remain the same.

Now let us examine temperature and heat flux profiles. The temperature $\langle\theta\rangle$ averaged across the cells is the sum of the reference conduction temperature $T(z, t)$ and the perturbation temperature $\langle\theta'\rangle$. Figure 2a shows the profiles of $T(z, t)$, $\langle\theta'\rangle$, and $\langle\theta\rangle$ at $t = 150$ when the cells reach a quasi-steady state. Except near the surface boundary, the total temperature $\langle\theta\rangle$ is uniformly distributed with depth as $\langle\theta'\rangle$ due to the cells offsets $T(z, t)$.

The total downward heat flux can be decomposed into two parts as $Q_t = Q_c + Q_a$, where the conductive heat flux Q_c is given by

$$Q_c = C_p\rho_w\kappa_T\frac{\partial\langle\tilde{\theta}\rangle}{\partial\tilde{z}} = Q\frac{\partial\langle\theta\rangle}{\partial z}$$

$$= Q\left(\frac{dT}{dz} + \frac{\partial\langle\theta'\rangle}{\partial z}\right) = Q_{c1} + Q_{c2}, \quad (34)$$

and the advective heat flux downward is given by

$$Q_a = -C_p\rho_w\langle\tilde{w}\tilde{\theta}'\rangle = -Q\frac{\mathrm{Pr}}{\mathrm{La}}\langle w\theta'\rangle. \quad (35)$$

The total heat flux Q_t has its maximum value Q at the surface and decreases with depth (Fig. 2b) because of continual surface cooling and a gradual decrease in temperature. The advective heat flux Q_a brings warm water up at the upwelling site and cold water down at the downwelling site and dominates the contribution to Q_t away from the upper and lower boundaries. As shown in Fig. 2c, the conductive heat flux Q_c is greatly reduced because of the temperature homogenization. Thus, the cells carry most of the heat flux through advection and reduce the conductive heat flux by homogenizing the temperature.

The flow patterns shown in Fig. 1 appear to be rather laminar, in contrast with highly turbulent flows expected in the ocean mixed layer. Unfortunately, it is impossible with our existing computing resources to resolve the turbulence, which is parameterized here through eddy-mixing coefficients. The effective Reynolds number, defined as $\mathrm{Re} = \tilde{w}_{\mathrm{dn}}d/\nu_T$ in which $\tilde{w}_{\mathrm{dn}}$ is the maximum downwelling velocity and d is the depth of the cells, is 120 for the numerical run presented in this section.

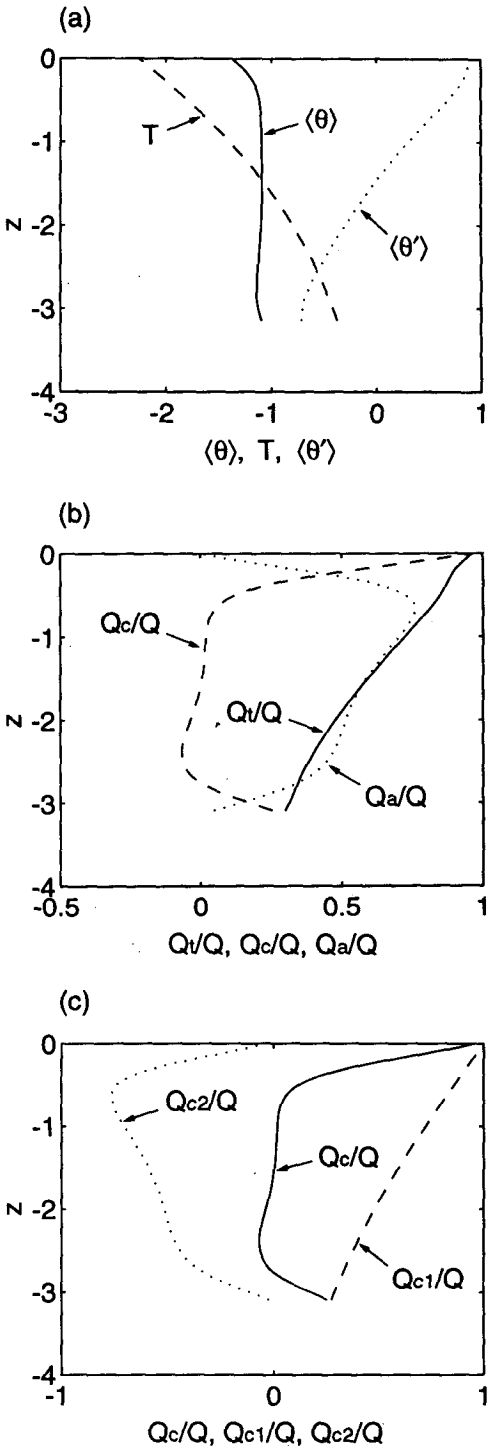

FIG. 2. Vertical profiles at La = 0.02, Ho = 0.05, and Pr = 1 for (a) temperature, (b) heat fluxes, and (c) conductive heat fluxes.

Unauthenticated | Downloaded 09/29/22 10:50 AM UTC

b. Transition from wave forcing to convective forcing

We have shown that the circulation is marginally reinforced by the convective force at Ho = 0.05. Our next step is to determine the critical value Ho_c at which the convective forcing becomes comparable to the wave forcing in driving Langmuir circulation. To do this, we examine the distributions of the three flow indices $\tilde{w}_{dn}$, Pt, and $\delta\tilde{\theta}$ as functions of La and Ho. The effects of varying Prandtl number Pr will be discussed in section 3d; for the moment we take Pr = 1.

Figure 3a summarizes the numerical results for the maximum downwelling velocity $\tilde{w}_{dn}$. As expected, $\tilde{w}_{dn}$ increases as La decreases. At a fixed value of La, $\tilde{w}_{dn}$ increases with increasing Ho. Thus, the circulation will be stronger when more convective forcing is added. Using a spline fit, we construct a three-dimensional distribution of $\tilde{w}_{dn}$ in La and Ho space, as shown in Fig. 3b. The strength of circulation as measured by $\tilde{w}_{dn}$ increases with the weakening of viscous dissipation and reinforcement of convective forcing.

We plot the pitch Pt as a function of La for different values of Ho in Fig. 4a. The pitch decreases as La is reduced and decreases with increasing Ho. The pitch appears to be a strong function of Ho but a weak function of La at small La. A corresponding three-dimensional diagram for Pt is shown in Fig. 4b.

Figure 5 shows the surface temperature anomaly across a cell as a function of La and Ho. For all three values of Ho, $\delta\tilde{\theta}$ shows the same trend, gently increasing with decreasing La (i.e., with decreasing viscosity). While $\delta\tilde{\theta}$ is a weak function of La, it is a strong function of Ho ($\delta\tilde{\theta}$ is approximately a linear function of Ho for small Ho, as expected if $\tilde{\theta}$ is a passive tracer of the flow and does not influence it dynamically). The functional dependence of $\delta\tilde{\theta}$ on the three dimensionless parameters will be further studied in section 3d.

Since the maximum downwelling velocity measures the strength of Langmuir circulation, we use it to classify the flows into two regimes: one dominated by wave forcing and the other dominated by convective forcing. We examine $\tilde{w}_{dn}$ in La and Ho space, and locate a dividing line at which $\tilde{w}_{dn}$ for the combined forcing is twice of that for wave forcing only (Fig. 6). Below this line, one can say that Langmuir circulation is dominated by wave forcing; above the line, the circulation is dominated by convective forcing. The critical value Ho_c is close to zero at large La where wave forcing alone cannot overcome viscous dissipation in causing convective instability. As La is reduced, Ho_c increases and approaches 3 at La = 0.01.

c. Scale analysis for Ho_c

As demonstrated in our numerical modeling, cells develop a boundary-layer structure similar to that observed in homogeneous water (LG). Figure 1 clearly shows the existence of a surface boundary layer and a narrow downwelling region in a cell. To exploit this,

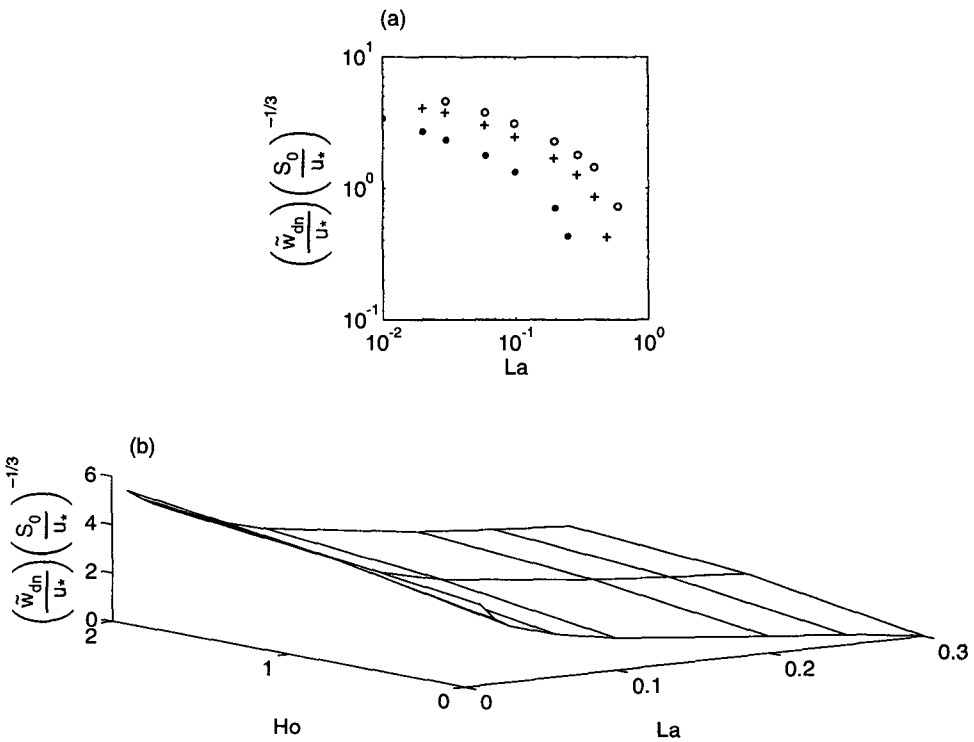

FIG. 3. Maximum downwelling velocity as a function of La and Ho. (a) Summary of numerical results for Ho = 0 (●), Ho = 1 (+), and Ho = 2 (○). (b) Three-dimensional distribution obtained from a spline fit.

Unauthenticated | Downloaded 09/29/22 10:50 AM UTC

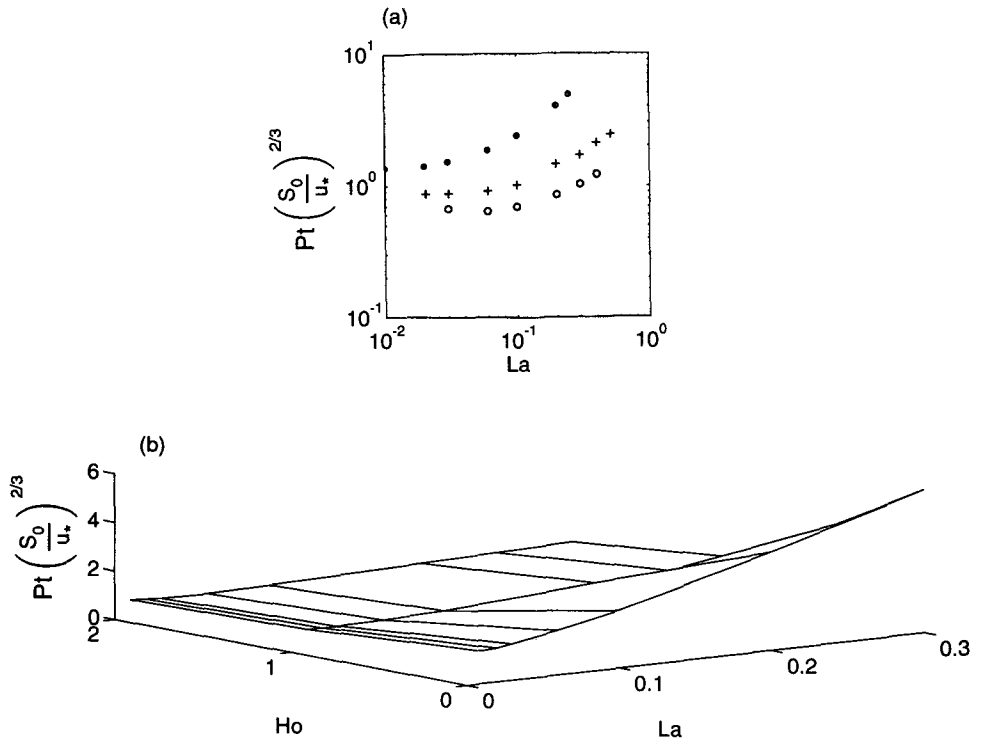

FIG. 4. Pitch distribution in La and Ho parameter space. (a) Summary of numerical results for Ho = 0 (●), Ho = 1 (+), and Ho = 2 (○); (b) three-dimensional distribution obtained from a spline fit.

we extend the scaling analysis developed in LG to study the small La regime. Our goal is to understand the critical value Ho_c determined in the numerical modeling and to determine the parametric dependence of key quantities.

The steady-state nondimensionalized governing equations are

$$v\frac{\partial u'}{\partial y} + w\left(\frac{\partial u'}{\partial z} + \frac{dU}{dz}\right) = \mathrm{La}\nabla^2 u', \tag{36}$$

$$v\frac{\partial \Omega}{\partial y} + w\frac{\partial \Omega}{\partial z} = \mathrm{La}\nabla^2\Omega - \frac{du_s}{dz}\frac{\partial u'}{\partial y} - \mathrm{Ho\ Pr}\frac{\partial \theta'}{\partial y}, \tag{37}$$

$$v\frac{\partial \theta'}{\partial y} + w\left(\frac{\partial \theta'}{\partial z} + \frac{dT}{dz}\right) = \frac{\mathrm{La}}{\mathrm{Pr}}\nabla^2\theta', \tag{38}$$

$$v = -\frac{\partial \psi}{\partial z}, \quad w = \frac{\partial \psi}{\partial y}, \quad \Omega = \nabla^2\psi, \tag{39}$$

where $dU/dz = \mathrm{erfc}(-z/(2\sqrt{\mathrm{La}t}))$ and $dT/dz = \mathrm{erfc}[-z/(2\sqrt{\mathrm{La}t/\mathrm{Pr}})]$. In the following analysis, we shall restrict our attention to Pr = 1. The length scales in the y and z directions are denoted by Y and Z, respectively; Ψ is chosen to represent the scale for streamfunction ψ; W is the scale of the downwelling velocity; U' is the scale of the perturbation downwind current u'; and T' represents the scale of the perturbation temperature θ'.

Within the narrow downwelling zone, the length scale in the y direction is much smaller than in the z direction, so that the viscous term is dominated by the horizontal component; that is, $\partial^2/\partial y^2 \gg \partial^2/\partial z^2$. As in LG, we hypothesize that the advective, diffusive, and forcing terms are of the same order of magnitude.

Equating advection and diffusion terms in the three equations gives

$$\Psi = \frac{\mathrm{La}Z}{Y}. \tag{40}$$

Balancing advection terms and forcing terms in (36) and (38) yields

$$U' = Z = \mathrm{O}(1), \quad T' = Z = \mathrm{O}(1), \tag{41}$$

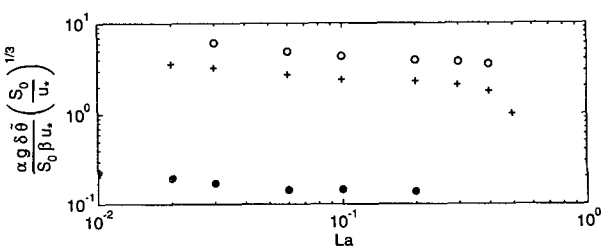

FIG. 5. Temperature anomaly as a function of La for Ho = 0.05 (●), Ho = 1 (+), and Ho = 2 (○).

Unauthenticated | Downloaded 09/29/22 10:50 AM UTC

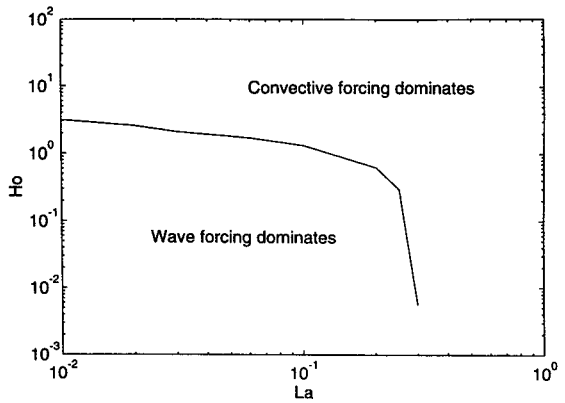

FIG. 6. The separation of the wave-forcing-dominated regime from the convection-dominated regime in La, Ho space. The solid line corresponds to $\tilde{w}_{dn}$ being doubled from its value at Ho = 0.

by taking $dU/dz = dT/dz = 1$. The same balance in (37) gives

$$\frac{\mathrm{La}^2 Z}{Y^5} = \frac{4U' + \mathrm{Ho}T'}{Y}. \tag{42}$$

Combining these relations and taking the dimensionless vertical scale as 1 gives

$$\Psi = (4 + \mathrm{Ho})^{1/4}\,\mathrm{La}^{1/2}, \tag{43}$$

$$W = (4 + \mathrm{Ho})^{1/2}, \tag{44}$$

$$Y = (4 + \mathrm{Ho})^{-1/4}\,\mathrm{La}^{1/2}. \tag{45}$$

Using (30), we infer for the dimensional downwelling velocity

$$\tilde{w}_{dn} \propto (4 + \mathrm{Ho})^{1/2}\,\mathrm{La}^{-1/3}. \tag{46}$$

Hence, one might deduce that the maximum downwelling velocity is doubled at $\mathrm{Ho}_c = 12$. This value is four times as large as the numerical value of $\mathrm{Ho}_c = 3$ at La = 0.01. However, in the scaling analysis we have used the surface value of the Stokes drift gradient to represent the magnitude of wave forcing. The discrepancy between the scale analysis and numerical modeling suggests that the vertical profile of wave forcing, ignored in the scaling analysis, is important. To check this, we have investigated the circulation driven solely by wave forcing. We have found that the maximum downwelling velocity $(\tilde{w}_{dn})_{lin}$ corresponding to a linear Stokes drift profile $du_s/dz = 4$ is about twice as big as $(\tilde{w}_{dn})_{exp}$ corresponding to the exponential profile $du_s/dz = 4e^{2z}$. If α is used to represent the magnitude of the exponential Stokes drift gradient in the vorticity equation, the scaling analysis tells us that $(\tilde{w}_{dn})_{exp} \propto \alpha^{1/2}$. Since $(\tilde{w}_{dn})_{exp}/(\tilde{w}_{dn})_{lin} = 0.5$, one deduces $(\alpha/4)^{1/2} = 0.5$. Thus we should use $\alpha = 1$ instead of 4 as the coefficient of U' in (42) in order to take the profile of the Stokes drift into account. If this is factored into the scaling analysis, we deduce $\mathrm{Ho}_c = 3$ at the point at which the transition from wave forcing to thermal forcing occurs, in good agreement with the numerical result.

d. *Effects of* Pr

So far we have assumed Pr = 1. This is not an unreasonable assumption for turbulent fluids, but it is interesting to see how our results vary with Pr. When Pr $\neq$ 1, the diffusion coefficients in the momentum and temperature equations are different. Therefore, when boundary layers develop at the surface and at the downwelling site, the thickness of thermal boundary layers differs from that of momentum boundary layers, as shown in Fig. 7.

In Fig. 8 the three flow indices for three values of Pr are compared at Ho = 1. The maximum downwelling $\tilde{w}_{dn}$ is an increasing function of Pr for large La (see Fig. 8a) because in this viscous regime the buoyancy forcing is strengthened by the weaker temperature diffusion at larger Pr. The temperature anomaly across a cell varies inversely with the thickness of the thermal boundary layer and hence is an increasing function of Pr, as shown in Fig. 8c. The remarkable thing to notice from this figure is that both $\tilde{w}_{dn}$ and Pt appear to be independent of Pr in the small La limit. This is because at Ho = 1 the circulation is driven primarily by wave forcing even when Pr exceeds 1. We have also analyzed the Pr dependence at Ho = 0.05 and found again that Pr has little influence on $\tilde{w}_{dn}$ and Pt. Thus, we conclude that wave forcing dominates over thermal convection in driving Langmuir circulation, irrespective of the choice of Pr.

For the small Ho of typical oceanic conditions, temperature is a passive tracer and the buoyancy forcing

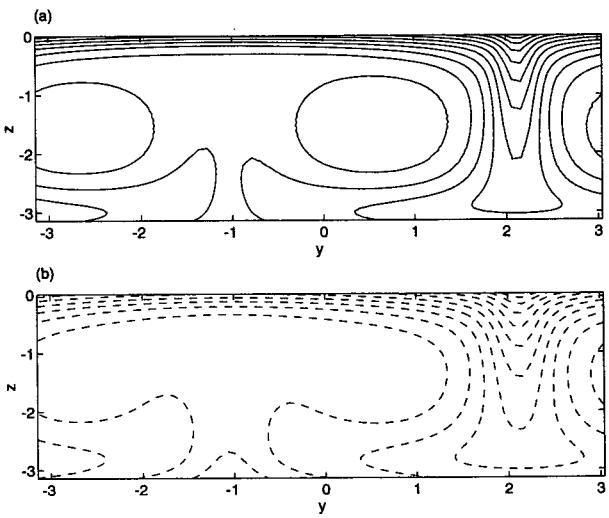

FIG. 7. Contours of (a) downwind current and (b) temperature at La = 0.02, Ho = 1, and Pr = 0.5 showing the differences in thickness of thermal and momentum boundary layers at the surface and in the downwelling region.

Unauthenticated | Downloaded 09/29/22 10:50 AM UTC

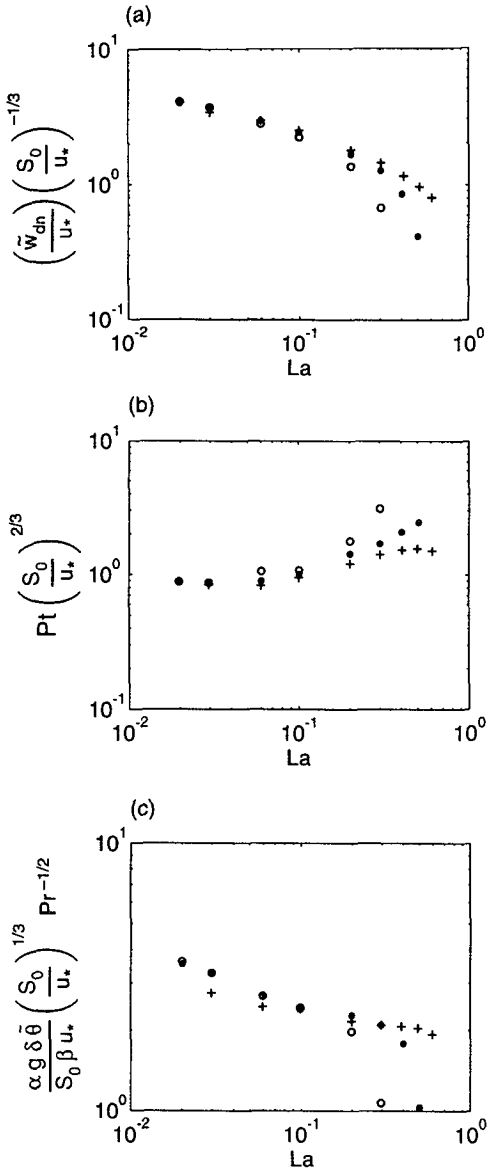

FIG. 8. Effects of Pr on three key flow quantities at Ho = 1 and for Pr = 0.5 (O), Pr = 1 (●), and Pr = 2 (+): (a) maximum downwelling velocity, (b) pitch, and (c) surface temperature anomaly.

makes a negligible contribution to the circulation strength, so that $\delta\tilde{\theta} \propto$ Ho. We can carry out a scale analysis of the governing equations for the surface boundary layer to deduce the full functional dependence of $\delta\tilde{\theta}$ on Ho, Pr, and La.

Mass conservation across the streamlines in a cell requires $\Psi = \mathrm{La}^{1/2}$ in the surface boundary layer, by use of (43) for small La. Comparability of advection and diffusion terms in (36) and (37) produces

$$Z_1 = \mathrm{La}^{1/2}, \tag{47}$$

where Z_1 is the thickness of the surface momentum layer.

When Pr $\neq$ 1, the thermal boundary layer has a different thickness, say Z_2. Suppose $\delta\theta$ represents the order of magnitude of the change of total temperature θ in the surface layer, either from the surface divergence to convergence or, equivalently, from the cell interior to the surface at a representative horizontal position. Since the heat flux is fixed at the surface, we have

$$\frac{\delta\theta}{Z_2} = 1. \tag{48}$$

Integration of the temperature equation across the surface layer yields

$$\frac{\Psi}{Z_1}\,\delta\theta Z_2 = \frac{\mathrm{La}}{\mathrm{Pr}}. \tag{49}$$

Combining with (48) and using the estimates of Ψ and Z_1, we deduce

$$\delta\theta \propto \mathrm{Pr}^{-1/2}\mathrm{La}^{1/2}. \tag{50}$$

Fitting to the numerical estimates of $\delta\theta$ at Ho = 0.05 for different values of Pr and La, and using (33) for dimensional $\delta\tilde{\theta}$, we derive

$$\delta\tilde{\theta} = c\frac{S_0\beta u_*}{\alpha g}\left(\frac{S_0}{u_*}\right)^{-1/3} \mathrm{Ho}\,\mathrm{Pr}^{1/2}\,\mathrm{La}^{-1/6}, \tag{51}$$

where $c \approx 2$ is the constant of proportionality. Formula (51) is equally applicable to the case when Ho is small and negative. Figure 8c shows that $\delta\tilde{\theta}\mathrm{Pr}^{-1/2}$ collapses at small La even for Ho = 1, but better agreement between (51) and numerical estimates is obtained at Ho = 0.05. We can extend the scale analysis to examine the effect of horizontally variable eddy viscosity and diffusivity. It can be shown that $\delta\tilde{\theta}$ only depends on the Prandtl number in the surface layer.

4. Suppression of circulation by heating

To consider the stratification effect caused by heating, we first investigate a surface heat flux and then a heat flux distributed with depth. It must be noted that Ho is now negative. In this section we shall fix Pr = 1.

a. Structure of flow and temperature fields

To illustrate the effects of surface heating, we present in Fig. 9 the snapshots of downwind current and vorticity fields when the cells are in a quasi-steady state. The dimensionless parameters are chosen to be La = 0.02, Ho = −1, and Pr = 1. In this case, the nondimensionalized temperature and downwind current are identical fields. Evidently the cells are constrained to a surface layer, which only occupies about one-third of the box depth. Much weaker circulatory cells are found at lower depths. In the surface layer the isolines of downwind current and temperature have a structure reminiscent of that seen in Fig. 1. Beneath the surface layer the isolines become almost horizontal. The vortex

Unauthenticated | Downloaded 09/29/22 10:50 AM UTC

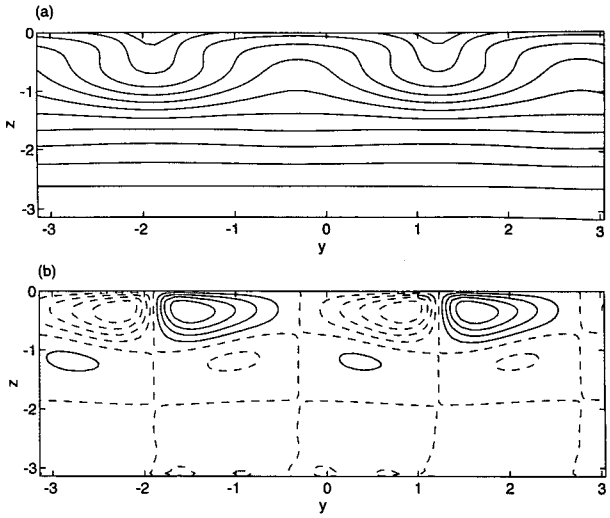

FIG. 9. Contours of downwind current and vorticity at La = 0.02, Ho = −1, and Pr = 1, illustrating the effect of stratification to constrain the vertical penetration of cells: (a) downwind current and (b) streamwise vorticity.

force overcomes stratification in the surface layer, but both $(du_s/dz)(\partial u/\partial y)$ and $\alpha\partial\theta/\partial y$ diminish at greater depth. These results show that strong surface heating inhibits the vertical penetration of Langmuir cells.

It is worth noting that four cells are left in the final quasi-steady state, in contrast to the two cells in the unstratified flow. When faced with strong surface heating, cell growth is limited by stratification but the cell aspect ratio remains about 1. However, for the physically plausible range of $-0.1 < \text{Ho} < 0$, we found that in the quasi-steady state, two cells filled the computational box with θ behaving as a passive tracer only.

Figure 10 illustrates the temperature and heat flux profiles for Ho = −1. Again we see that temperature is homogenized in the surface layer occupied by the strongest cells (Fig. 10a). Below the surface layer the temperature is mainly conducted downward, although a small portion is carried by the weaker cells situated there. Both conduction and advection contribute to a heat flux that tends to cool the surface water and warm the cold water below (Fig. 10b). Figure 10c shows that advection carries most of the heat flux in the middepths of the surface cells.

b. *The stability diagram in* La, Ho *space*

The above example demonstrates that the stratification induced by strong surface heating suppresses the circulation driven by surface waves. Figure 11 summarizes the magnitude of maximum downwelling velocity $\tilde{w}_{\text{dn}}$ as a function of La and Ho. Clearly $\tilde{w}_{\text{dn}}$ increases with decreasing values of La but becomes smaller if Ho decreases. It is expected that the circulation will be completely inhibited at Ho between −2 and −4, although the precise value of Ho is somewhat tedious to pin down because cells take a long time to develop when the parameters are close to the stability boundary.

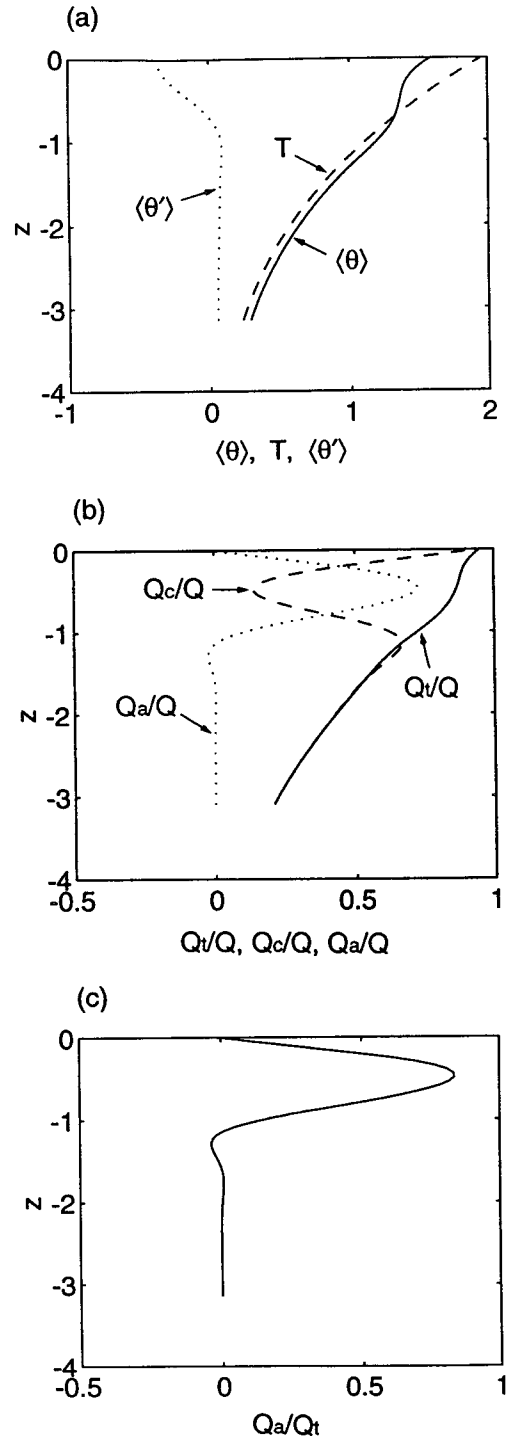

FIG. 10. Vertical profiles at La = 0.02, Ho = −1, and Pr = 1 for (a) temperature, (b) heat fluxes, and (c) the ratio Q_a/Q_t.

Unauthenticated | Downloaded 09/29/22 10:50 AM UTC

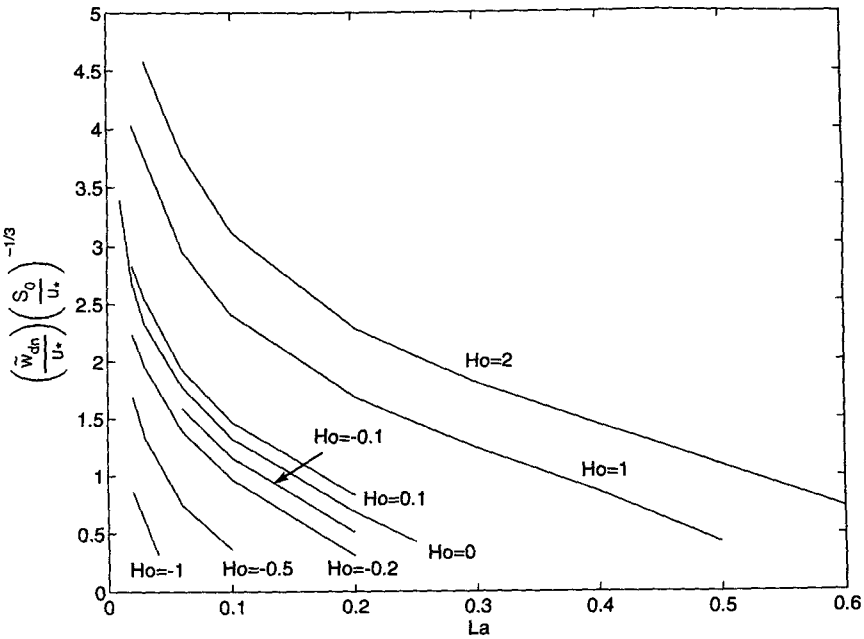

FIG. 11. The effect of stratification on the maximum downwelling velocity: Ho > 0 represents surface cooling, while Ho < 0 represents surface heating.

Nevertheless, it is worthwhile to map out the stability boundary in the La and Ho space. Using the value of the maximum downwelling velocity, we extrapolate the critical value of La_c at which the cells just become unstable for each value of Ho. We have tried to push La against the critical value as much as possible and believe our estimate of La_c is accurate, although mapping out the precise stability boundary requires a proper stability analysis, which will not be attempted in this paper. Figure 12 shows the stability diagram, and it is clear that the critical value La_c at which instability develops is an increasing function of Ho. With Ho < 0 surface heating suppresses the instability, while with Ho > 0 surface cooling reinforces the instability.

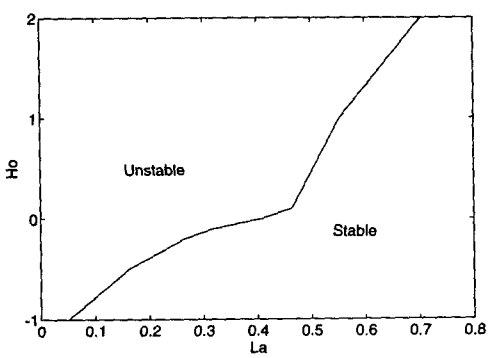

FIG. 12. The stability diagram in La/Ho space at Pr = 1. The critical value La_c is estimated by extrapolating $\tilde{w}_{dn}$ to the La at which it is zero.

c. *Small effects of a typical surface heat flux*

We have seen some striking effects of buoyancy flux on Langmuir cells. Given a typical value of the surface heat flux, a problem of practical concern is whether the stratification will strongly damp the circulation. The heat flux during daytime heating is usually no more than 1000 W m^{-2}. Hence, Ho = −0.1 represents an upper limit under moderate winds. Numerical results show that for small La, the reduction in downwelling velocity is 5% and the amplification of pitch is 8%. There is a larger reduction in $\tilde{w}_{dn}$ at larger values of La when Langmuir circulation is relatively weak due to strong viscous dissipation. As the circulation becomes more vigorous, the surface heating has little impact on the vertical velocity. Furthermore, we notice no appreciable effect of the buoyancy flux on the pitch in the small La regime. The mismatch of pitch between the CL model and observations (see LG) does not become smaller when the effect of surface buoyancy flux is included.

Thorpe and Hall (1982) and Weller and Price (1988) reported a small and positive temperature difference between the surface convergence and divergence lines ($-\delta\tilde{\theta}$) of 0.005 and 0.015 K under strong winds. The positive temperature anomaly, with water at convergence warmer than at divergence, was presumably measured during the periods when the ocean received a net heat flux (i.e., $Q > 0$). Taking the maximum Q = 500 W m^{-2} and maximum U_w = 15 m s^{-1} recorded during the experiment, we estimate Ho = −0.023. The model predicts a positive surface temperature anomaly

Unauthenticated | Downloaded 09/29/22 10:50 AM UTC

of 0.012 K at Pr = 1, which falls into the range of the observed values. The agreement is encouraging but inconclusive because $\delta\tilde{\theta}$, while rather insensitive to La in (51), is proportional to $\mathrm{Pr}^{1/2}$, and we do not know the eddy Prandtl number of the flow. Another factor that might affect the prediction of $\delta\tilde{\theta}$ is the heat flux through the base of the mixed layer, which is not considered in this model.

d. Solar insolation distributed with depth

The model assumes that the incoming solar radiation Q_s is absorbed at the water surface. In reality only about 55% of Q_s is absorbed very close to the surface; the remainder penetrates deeper and is absorbed more or less exponentially. The attenuation coefficient γ varies between about 0.03 m^{-1} in clear Mediterranean water and 0.3 m^{-1} in dirty coastal water. A value of 0.04 m^{-1}, corresponding to a scale depth of 25 m, appears to characterize much of the open tropical and subtropical oceans (Niiler and Kraus 1977).

Our model can easily be modified to study the effect of a distributed heat flux. Assuming all the heat flux to be distributed with depth, the nondimensionalized governing equations obtained are

$$\frac{\partial u}{\partial t} + v\frac{\partial u}{\partial y} + w\frac{\partial u}{\partial z} = \mathrm{La}\nabla^2 u, \tag{52}$$

$$\frac{\partial \Omega}{\partial t} + v\frac{\partial \Omega}{\partial y} + w\frac{\partial \Omega}{\partial z} = \mathrm{La}\nabla^2\Omega - \frac{du_s}{dz}\frac{\partial u}{\partial y} - \mathrm{Ho\,Pr}\frac{\partial \theta}{\partial y}, \tag{53}$$

$$\frac{\partial \theta}{\partial t} + v\frac{\partial \theta}{\partial y} + w\frac{\partial \theta}{\partial z} = \frac{\mathrm{La}}{\mathrm{Pr}}\left(\nabla^2\theta + \frac{dQ}{dz}\right), \tag{54}$$

$$v = -\frac{\partial \psi}{\partial z}, \quad w = \frac{\partial \psi}{\partial y}, \quad \Omega = \nabla^2\psi, \tag{55}$$

where the internal heating rate is determined by $Q = \exp(\gamma z/\beta)$. The surface boundary conditions are

$$\frac{\partial u}{\partial z} = 1, \quad \frac{\partial \theta}{\partial z} = 0, \quad \psi = \frac{\partial^2 \psi}{\partial z^2} = 0. \tag{56}$$

Usually the scale depth $1/\gamma$ of the solar insolation is much greater than the e-folding depth $1/(2\beta) = 0.12U_w^2/g$ of the Stokes drift, which is 2.76 m for $U_w = 15$ m s^{-1}. In the following simulations, we investigate the influence of $d_r = (2\beta)/\gamma$, the ratio of the solar attenuation depth to the Stokes drift e-folding depth, with $d_r = 10$ being a typical value. The computational box chosen in our simulations has a size of $\beta L = 2\pi$ and $\beta d = \pi$, corresponding to a width of 34 m and a depth of 17 m at wind speed of 15 m s^{-1}.

The maximum downwelling velocity corresponding to distributed heating $Q\exp(\gamma\tilde{z})$ is compared with that for the same heat flux Q applied at the surface. We choose Ho = −0.1, a typical value for the incoming solar radiation alone, and study four different attenuation depths as measured by d_r. Our numerical results show that $\tilde{w}_{\mathrm{dn}}$ for the distributed heating is slightly larger than that for the surface heating, approaching the downwelling velocity without incoming heat flux when d_r becomes large, so that distributed heating has even less impact on the strength of Langmuir circulation than surface heating.

Figure 13 shows a strong dependence of $\delta\tilde{\theta}$ on d_r. The temperature anomaly is reduced to one-third for $d_r = 1$ and by a factor of 70 for $d_r = 10$. As the incoming heat flux is distributed over a greater depth, the water is closer to being homogeneous and the temperature anomaly is reduced. In turn, this will exert less buoyancy torque on the water, further failing to constrain the circulation. It is noted that $|\delta\tilde{\theta}|$ gently decreases with decreasing La for $d_r = 2$, 5, 10, in contrast with the case $d_r = 1$ when $|\delta\tilde{\theta}|$ starts to grow at a small La. It is possible that, for high values of d_r, $|\delta\tilde{\theta}|$ will start to increase at much smaller La, though further numerical runs will not add much to the point already made regarding the weak dependence of $\delta\tilde{\theta}$ on La.

We have demonstrated that $\delta\tilde{\theta}$ associated with the internal heating is negligible for a typical d_r. The temperature anomaly across Langmuir cells must then be induced by the heat flux coming through the surface, which accounts for 55% of the insolation. When using (51) to predict the temperature anomaly for $Q > 0$, we must base Ho on the heat flux that is absorbed or lost right at the surface.

5. Conclusions

We have investigated subsurface Langmuir circulation driven by surface waves as well as by surface cooling. It is found that the vortex force of surface

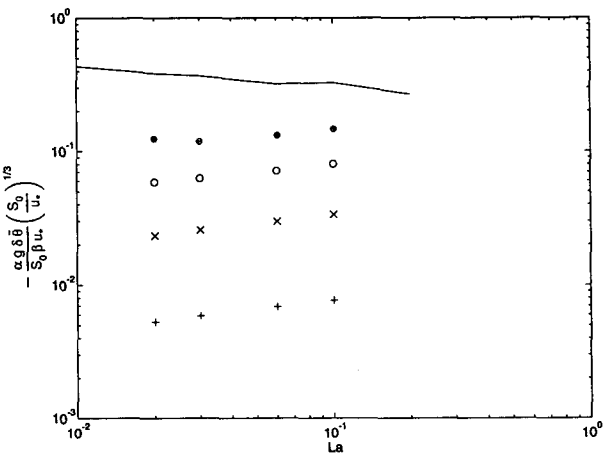

FIG. 13. Effects of a distributed heat flux on the temperature anomaly for Ho = −0.1. The solid line corresponds to a surface heat flux. Points ● (d_r = 1), ○ (d_r = 2), × (d_r = 5), and + (d_r = 10) represent distributed heating.

Unauthenticated | Downloaded 09/29/22 10:50 AM UTC

waves proposed in the CL model typically dominates over thermal forcing in driving the circulation.

Under moderate winds, typical surface heating or cooling does not significantly alter the dynamics of the CL model. Strong cells prevent any stratification from forming, so that the pitch predicted by the CL model does not get closer to the observed values. The addition of a convective forcing makes the theoretical pitch even less. Thus, the inclusion of buoyancy flux cannot bridge the apparent gap in the pitch between the CL model and observations.

For a given heat flux, the temperature difference between the regions of surface divergence and convergence in Langmuir circulation depends on Ho, Pr, and La and on the depth distribution of the heating but is typically $O(10^{-2})$ K, falling into the range of observed values, although the difficulty in estimating the eddy Prandtl number makes the comparison between the model and observations uncertain.

In our model we assume that the circulation is composed of two-dimensional cells with their axes aligned in the wind direction. Although observations of atmospheric convective rolls suggest that the rolls usually align with the wind direction, Soloviev (1990) and Thorpe et al. (1991) observed temperature ramps in a crosswind direction in a thermally unstable ocean surface layer. Further theoretical studies may require the consideration of these three-dimensional convective plumes, although their main role may be to increase the eddy mixing coefficients.

Future studies will address the effect of Langmuir circulation on a preexisting stratification, and particularly the mechanism by which a surface mixed layer is deepened.

Acknowledgments. We thank Craig Gilman, Johannes Gemmrich, and Amit Tandon for helpful discussions and Bob Weller for useful comments on a draft. Thanks are also due to Rosalie Rutka for editorial assistance. Financial support from the U.S. Office of Naval Research and Canada's Natural Sciences and Engineering Research Council is gratefully acknowledged.

REFERENCES

Batchelor, G. K., 1956: On steady laminar flow with closed streamlines at large Reynolds number. *J. Fluid Mech.*, **1,** 177–190.

Craik, A. D. D., 1977: The generation of Langmuir circulations by an instability mechanism. *J. Fluid Mech.*, **81,** 209–223.

——, and S. Leibovich, 1976: A rational model for Langmuir circulations. *J. Fluid Mech.*, **73,** 401–426.

Csanady, G. T., 1965: Windrow studies. Rep. PR26, Great Lakes Institute, University of Toronto, Ontario, 82 pp.

Domaradzki, J. A., and R. W. Metcalfe, 1988: Direct numerical simulations of the effects of shear on turbulent Rayleigh–Bénard convection. *J. Fluid Mech.*, **193,** 499–531.

Etling, D., and R. A. Brown, 1993: Roll vortices in the planetary boundary layer: A review. *Bound.-Layer Meteor.*, **65,** 215–248.

Kuettner, J. P., 1971: Cloud bands in the earth's atmosphere. *Tellus,* **23,** 404–425.

Kuo, H., 1963: Perturbations of plane Couette flow in stratified fluid and origin of cloud streets. *Phys. Fluids,* **6,** 195–211.

Langmuir, I., 1938: Surface motion of water induced by wind. *Science,* **87,** 119–123.

Large, W. G., and S. Pond, 1982: Sensible and latent heat flux measurements over the ocean. *J. Phys. Oceanogr.*, **12,** 464–482.

Leibovich, S., 1977: Convective instability of stably stratified water in the ocean. *J. Fluid Mech.*, **82,** 561–581.

——, 1983: The form and dynamics of Langmuir circulations. *Ann. Rev. Fluid Mech.*, **15,** 391–427.

——, and K. Radhakrishnan, 1977: On the evolution of the system of wind drift currents and Langmuir circulations in the ocean. *J. Fluid Mech.*, **80,** 481–507.

Li, M., and C. Garrett, 1993: Cell merging and jet/downwelling ratio in Langmuir circulation. *J. Mar. Res.*, **51,** 737–769.

Niiler, P. P., and E. B. Kraus, 1977: One-dimensional models of the upper ocean. *Modelling and Prediction of the Upper Layers of the Ocean,* E. B. Kraus, Ed., Pergamon, 143–172.

Rhines, P. B., and W. R. Young, 1982: Homogenization of potential vorticity in planetary gyres. *J. Fluid Mech.*, **122,** 347–367.

Shay, T. J., and M. C. Gregg, 1986: Convectively driven turbulent mixing in the upper ocean. *J. Phys. Oceanogr.*, **16,** 1777–1798.

Smith, S. D., 1988: Coefficients for sea surface wind stress, heat flux, and wind profiles as a function of wind speed and temperature. *J. Geophys. Res.*, **93,** 15 467–15 472.

Soloviev, A. V., 1990: Coherent structures at the ocean surface in convectively unstable conditions. *Nature,* **364,** 157–160.

Thorpe, S. A., 1985: Small-scale processes in the upper ocean boundary layer. *Nature,* **318,** 519–522.

——, 1992: Bubble clouds and the dynamics of the upper ocean. *Quart. J. Roy. Meteor. Soc.*, **118,** 1–22.

——, and A. J. Hall, 1982: Observations of the thermal structure of Langmuir circulation. *J. Fluid Mech.*, **114,** 237–250.

——, M. Cure, and M. White, 1991: The skewness of temperature derivatives in oceanic boundary layers. *J. Phys. Oceanogr.*, **21,** 428–433.

Turner, J. S., 1973: *Buoyancy Effects in Fluids.* Cambridge University Press, 368 pp.

Vonnegut, K., 1963: *Cat's Cradle.* Gollancz, 191 pp.

Weller, R. A., and J. F. Price, 1988: Langmuir circulation within the oceanic mixed layer. *Deep-Sea Res.*, **35,** 711–747.

Unauthenticated | Downloaded 09/29/22 10:50 AM UTC